Proceedings of
11th European Conference on Turbomachinery Fluid dynamics & Thermodynamics
ETC11, March 23-27, 2015, Madrid, Spain

AN ALGEBRAIC INTERMITTENCY MODEL ADDED TO THE k-ω RANS MODEL FOR TRANSITION SIMULATION

S. Kubacki[1], B. Górecki[1], E. Dick[2]

[1]Institute of Aeronautics and Applied Mechanics, Warsaw University of Technology, Nowowiejska 24, 00-665, Warsaw, Poland; slawomir.kubacki@meil.pw.edu.pl
[2]Department of Flow, Heat and Combustion Mechanics, Ghent University, St.–Pietersnieuwstraat 41, 9000 Ghent, Belgium; erik.dick@ugent.be

ABSTRACT

A simple algebraic intermittency model is proposed for simulation of laminar to turbulent boundary layer transition under high free-stream turbulence. The intermittency model is combined with the newest version of the k-ω RANS turbulence model by Wilcox. The transition model takes into account, in an approximate way, two effects in an attached pre-transitional boundary layer: damping of short-wavelength disturbances caused by the free stream and breakdown of long-wavelength disturbances inside the boundary layer into fine-scale turbulence. The transition model uses only local variables.

The model has been tuned for the flat plate T3C cases of ERCOFTAC, relevant for bypass transition and tested for flow through cascades of N3-60 ($Re=6\cdot10^5$) vanes and T106A ($Re=1.6\cdot10^5$) blades. The transition model produces good results for bypass transition in attached boundary layers far from separation (2D RANS) and prone to separation (2D RANS and 3D URANS). Good results are also obtained for transition in separated laminar boundary layers (3D URANS) thanks to resolution of their instability and the onset of the breakdown.

NOMENCLATURE

f_{SS}	shear sheltering factor	S	shear rate magnitude
k	turbulent kinetic energy	Tu	turbulence intensity
k_s	small-scale turbulent kinetic energy	γ	intermittency factor
k_l	large-scale turbulent kinetic energy	ω	specific dissipation rate
		Ω	rotation rate magnitude

INTRODUCTION

Transition from laminar to turbulent state in turbomachinery boundary layer flows is influenced by free-stream turbulence and pressure gradient. With a turbulence level above 0.5 to 1 %, the free-stream turbulence induces streamwise elongated disturbances in the near-wall region of an attached laminar boundary layer, termed streaks or Klebanoff distortions. They are zones of forward and backward jet-like perturbations alternating in spanwise direction, with almost perfect periodicity. The Klebanoff disturbances grow downstream both in length and amplitude and finally break down with formation of turbulent spots. Transition is then called of bypass type, which means that the instability mechanism of the Tollmien-Schlichting waves is bypassed. The mechanisms of bypass transition were analysed by Jacobs and Durbin (2001), Brandt et al. (2004) and Zaki and Durbin (2005), among others. Klebanoff disturbances are initiated by deep penetration into the boundary layer of low-frequency perturbations from the free stream. High-frequency components are strongly damped by the boundary layer. This filtering effect by the boundary layer is called shear sheltering. It is the stronger the higher is the shear rate. There seem to be two mechanisms by which streaks may become unstable. One is Kelvin-Helmholtz instability of the inflectional wall-normal velocity

profile between low-speed streaks and the boundary layer edge. The other is a similar instability of the shear layers with inflectional spanwise velocity profiles in between low- and high-speed streaks. Both instabilities are triggered by high-frequency components in the free-stream turbulence. Due to the inviscid instability mechanism, the breakdown is much faster than with natural transition.

In a boundary layer with laminar separation and low free-stream turbulence, transition is initiated by inviscid Kelvin-Helmholtz instability of the laminar free shear layer, with formation of spanwise vortices. They group at selective streamwise wavelengths, analogous to Tollmien-Schlichting waves in an attached boundary layer (McAuliffe and Yaras 2010). The roll-up vortices break down as they travel downstream. The breakdown process is rather slow with low free-stream turbulence, but, under high free-stream turbulence, the process of bypass transition with formation of streaks in the pre-transitional attached boundary layer can co-exist with the Kelvin-Helmholtz generated spanwise vortices in the separated layer. The breakdown of the vortex rolls is then strongly accelerated by perturbations due to the Klebanoff modes. For sufficiently strong free-stream turbulence, the Kelvin-Helmholtz instability may even be bypassed by the breakdown of the streaks. So, a bypass mechanism is possible, similar as in an attached boundary layer.

TRANSITION MODEL FOR BYPASS TRANSITION

The algebraic intermittency model is combined with the newest version of the k-ω model by Wilcox (2008). The equations have been implemented in the FLUENT commercial CFD package with the UDF facility. The transport equations for turbulent kinetic energy and specific dissipation rate are

$$\frac{Dk}{Dt} = \gamma \nu_s S^2 - \beta^* k\omega + \frac{\partial}{\partial x_j}\left[\left(\nu + \sigma^* \frac{k}{\omega}\right)\frac{\partial k}{\partial x_j}\right], \tag{1}$$

$$\frac{D\omega}{Dt} = \alpha \frac{\omega}{k} \nu_s S^2 - \beta \omega^2 + \frac{\partial}{\partial x_j}\left[\left(\nu + \sigma \frac{k}{\omega}\right)\frac{\partial \omega}{\partial x_j}\right] + \frac{\sigma_d}{\omega}\frac{\partial k}{\partial x_j}\frac{\partial \omega}{\partial x_j}. \tag{2}$$

The intermittency factor γ (see later Eq. 7) is a multiplier of the production term in the k-equation. The production term is $\nu_s S^2$ where ν_s is the small-scale eddy viscosity (see later Eq. 6), which is part of the full eddy viscosity ν_T. S is the magnitude of the shear rate tensor $S = (2S_{ij}S_{ij})^{1/2}$, with components $S_{ij} = 1/2(\partial U_i/\partial x_j + \partial U_j/\partial x_i) - 1/3(\partial U_k/\partial x_k)\delta_{ij}$. The introduction of γ and ν_s are the only changes in the k-ω model. In the laminar part of a boundary layer, γ is set to zero. There is then no production of k, but turbulent kinetic energy enters by diffusion out of the free-stream flow. In the laminar part of a boundary layer, the ω-equation stays active. This is allowed since, as proven by Wilcox, the ω-equation has a nonzero laminar-flow solution for vanishing k and vanishing eddy-viscosity.

The turbulent kinetic energy k is split, based on the model for shear sheltering by Walters and Leylek (2004) and Walters and Cokljat (2008), into a small-scale part k_s and a large-scale part k_l as

$$k_s = f_{ss} k, \quad k_l = k - k_s. \tag{3}$$

The splitting expresses that high-frequency components of free-stream disturbances are damped in the outer part of a laminar boundary layer. Shear sheltering is filtering due to shear, whereby only low-frequency components of the free-stream turbulence can propagate deeply into a laminar boundary layer. Shear sheltering is determined by the relative importance of two time scales: the time scale of convection relative to an observer inside the shear layer and the time scale of wall-normal diffusion into the boundary layer. The convective time scale is obviously the time scale of the main strain $\tau_c = 1/\Omega$, where Ω is the magnitude of the vorticity tensor, i.e. $\Omega = (2\Omega_{ij}\Omega_{ij})^{1/2}$, with components $\Omega_{ij} = 1/2(\partial U_i/\partial x_j - \partial U_j/\partial x_i)$. The diffusive time scale is fundamentally ℓ_d^2/ν, with ℓ_d the

diffusive length scale and ν the kinematic fluid viscosity. For fluctuations in a laminar boundary layer, this length scale was estimated by Walters (2009), assuming proportionality between $\sqrt{k}/\ell_d$, where $\sqrt{k}$ is the velocity scale of the fluctuations, and the mean velocity gradient, which is Ω. This results in $\ell_d \sim \sqrt{k}/\Omega$ and $\tau_d \sim k/\nu\Omega^2$. The ratio of the diffusive and convective time scales forms the Reynolds number $k/\nu\Omega$. With this Reynolds number, Walters and Cokljat (2008) define a shear-sheltering factor, which we employ, by

$$f_{SS} = \exp[-(C_{SS}\,\nu\Omega/k)^2]. \qquad (4)$$

With the shear-sheltering factor, the turbulent kinetic energy of the turbulence that penetrates the pre-transitional boundary layer is split into a large-scale part and a small-scale part (Eq. 3). The large-scale or long-wavelength part is the part that reaches wall vicinity. This part causes the streaks. The small-scale part or short-wavelength part occurs near the edge of the boundary layer. Fluctuations in the streaks are dominantly unidirectional and can thus be characterized as laminar. In the modelling approach of Walters and Leylek (2004) and Walters and Cokljat (2008), this effect is expressed by two ingredients. One is that production of turbulence in the pre-transitional boundary layer is only due to the small-scale eddy viscosity (Eq. 1). We follow this description. The second is by writing an equation for laminar-fluctuation kinetic energy with a similar form as an equation for turbulent kinetic energy, but with a production term written with a large-scale eddy viscosity. We use the expressions of small-scale and large-scale eddy viscosities from their modelling approach, but we do not use an equation for laminar-fluctuation kinetic energy.

The eddy viscosity associated to large scales is calculated in the same way as the eddy viscosity of the original turbulence model (Wilcox 2008), but by replacing k by k_l:

$$\nu_l = \frac{k_l}{\tilde{\omega}}, \quad \text{with} \quad \tilde{\omega} = \max\left[\omega, C_{\lim}\sqrt{\frac{2S_{ij}S_{ij}}{\beta^*}}\right], \quad C_{\lim}=7/8. \qquad (5)$$

The small-scale eddy viscosity, used in the source terms of the turbulence equations, is

$$\nu_s = \beta^* k_s \tau_s \ , \quad \text{with} \quad \tau_s = \max\left(\tau_t, \tau_K\right) \ , \quad \text{where} \quad \tau_t = 1/\beta^*\tilde{\omega} \quad \text{and} \quad \tau_K = C_K(\nu/\varepsilon)^{1/2}. \quad (6)$$

The turbulent time scale is τ_t, but, because the small-scale turbulence contributing to the eddy viscosity may become very small in a separated shear layer, we do not allow that this time scale becomes smaller than the Kolmogorov scale τ_K, where C_K is a constant of order unity and $\varepsilon = \beta^* k\omega$. The resulting eddy viscosity, used in the Navier-Stokes equations is $\nu_T = \nu_s + \nu_l$.

In the approach of Walters and Leylek (2004) and Walters and Cokljat (2008), breakdown of laminar streaks and thus onset of transition is modelled by activation of a transfer term with negative sign in the equation of laminar-fluctuation kinetic energy and positive sign in the equation of turbulent kinetic energy. This transfer concept is also used in other models with laminar-fluctuation kinetic energy (e.g. Lardeau et al. 2004). A more classic approach is intermittency modelling. In a boundary layer with turbulent spots, the velocity at a fixed position in the boundary layer varies in time with alternating periods of high-frequency fluctuations during the passage of a spot, thus turbulent flow, and low-frequency perturbations in between spots, thus laminar flow. The flow is called intermittent, meaning that turbulent phases alternate with laminar phases. The fraction of time that the flow is turbulent is called the intermittency factor γ. In an intermittency modelling approach, breakdown of streaks, thus onset of transition, is described either by pre-multiplication of the eddy viscosity by the intermittency factor or by pre-multiplication of the production term in the equation for turbulent kinetic energy by the intermittency factor. The intermittency factor may be expressed algebraically or may be derived from one or two transport equations. A well-known intermittency model is the one by Menter et al. (Langtry and Menter 2009) with two dynamic

equations. But many other models exist, including models with two dynamic equations and one dynamic equation by the research groups of the present authors (Lodefier and Dick 2006, Kubacki et al. 2009). There is some relation between intermittency modelling and laminar-fluctuation kinetic energy modelling as intermittency may also be seen as the ratio of the turbulent kinetic energy to the sum of turbulent kinetic energy and laminar-fluctuation kinetic energy. We opt here for intermittency description because an intermittency factor can be described algebraically, therefore avoiding supplementary dynamic equations.

For the expression of the intermittency factor, we rely on the work of Praisner and Clark (2007), who showed that bypass transition starts when the time scale of the turbulent motion (τ_t) becomes smaller (thus faster breakdown) than the time scale of the boundary layer diffusion (τ_d). We take again the estimate of the diffusive time scale by Walters (2009). The ratio of τ_d to τ_t is proportional to $k\omega/(\nu\Omega^2)$ so that this quantity can be used for starting bypass transition. The intermittency factor γ is expressed by

$$\gamma = \min\left(\varsigma_T / A_T, 1\right), \quad \text{with} \quad \varsigma_T = \max\left(k\omega/\nu\,\Omega^2 - C_T, 0\right), \tag{7}$$

where C_T is a threshold value and A_T a growth rate.

The intermittency factor γ is zero in the inner part of a laminar boundary layer (say for y/δ<0.2). The damping factor f_{SS} (Eq. 4) is also small there. It means that small-scale freestream turbulence is suppressed by both γ and f_{SS} in the near-wall zone of a laminar boundary layer. The intermittency factor controls the small-scale turbulence production very near to the wall and is used to activate transition onset by Eq.7 (see later discussion). Only high-frequency disturbances (small-scales) can cause instability of Klebanoff distortions and so can initiate transition. This effect is accounted for by multiplying the small-scale production term in the k-equation with the shear-sheltering factor f_{SS}. So, both γ and f_{SS} have a role in the transition model. In a fully turbulent boundary layer both γ=1 and f_{SS}=1 over most of the boundary layer thickness. These factors remain zero very close to a wall, approximately in the viscous sublayer. The small-scale turbulent kinetic energy becomes equal to the total turbulent kinetic energy, except for the zone very near to a wall. The difference very near to a wall does not lead to alteration of the behaviour of the originating turbulence model in fully turbulent flow.

CALIBRATION OF THE BYPASS TRANSITION MODEL

The algebraic intermittency model contains 4 constants: C_T, A_T, C_{SS} and C_K (Table 1). C_T, A_T and C_{SS} control bypass transition in attached boundary layer state. These parameters have been tuned on three ERCOFTAC flat plate test cases of the T3C series, T3C2, T3C3 and T3C5, relevant for bypass transition. The parameter C_K has a role for transition in separated boundary layer state. The value of C_K has been determined by transition prediction in separated state on the T106A gas turbine profile at low turbulence level.

Steady 2D flow simulations of the T3C flat plates with sharp leading edges were performed with uniform profiles of velocity, k and ω at the inlet to the computational domain, located 0.05 m upstream of the leading edge (x=0). Grid spacing was uniform in streamwise direction. Grids were stretched in wall-normal direction, starting from cells at the wall with $y+$ value in the centre less than 0.2. The total number of cells was 50,000-70,000, depending on the case. The coupled pressure-based solver of Fluent was applied. The normalized residuals of the equations of momentum, k and ω were driven to below 10^{-6}. The inlet conditions are given in Table 2. The pressure gradient was imposed by an upper slip wall of the domain adjusted in order to reproduce the evolution of the free-stream mean velocity along the plate (Fig. 1). The upper wall was placed at distance 0.2m from the plate at x=0. The inlet value of ω was adjusted in order to reproduce the experimental decay of the free-stream turbulence intensity along the plate (Fig. 1). The agreement is good, which is crucial for proper tuning of the transition model.

Table 1. Transition model constants.

C_T	A_T	C_{SS}	C_K
0.1	1.0	2.5	1.5

Table 2. Flat plates. Boundary conditions at inlet to the computational domain.

Test case	Simulation	U [m/s]	k [m^2/s^2]	ω [$1/s^2$]	Transition zone
T3C2 (Tu=3.0%)	2D RANS	5.10	0.0380	280	Just after ZPG
T3C3 (Tu=3.0%)	2D RANS	3.65	0.0220	170	In decelerating flow
T3C5 (Tu=3.0%)	2D RANS	8.40	0.2100	760	In accelerating flow

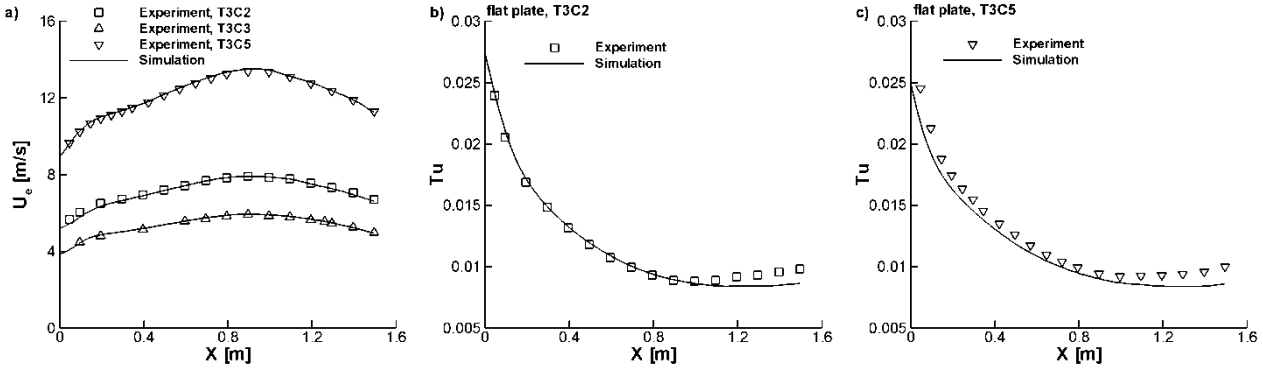

Fig. 1. T3C cases for tuning. Mean velocity (a) and turbulence intensity (b and c) at the edge of the boundary layer (turbulence intensity is similar for T3C3 but not shown).

Fig. 2 shows skin friction along the plates by the steady RANS k-ω model supplemented with the algebraic transition model. Onset of transition can be tuned rather well with a single value of C_T, but the transition zone is always too short. We show later that the much too abrupt transition for the tuning cases has only a small effect on the results of the flow through the N3-60 (2D RANS) and T106A (2D RANS and 3D URANS) cascades at high free-stream turbulence. Therefore, we decided for this first study of the transition model not to put effort in improving the length of the transition zone and we set somewhat arbitrarily the growth rate factor A_T to unity.

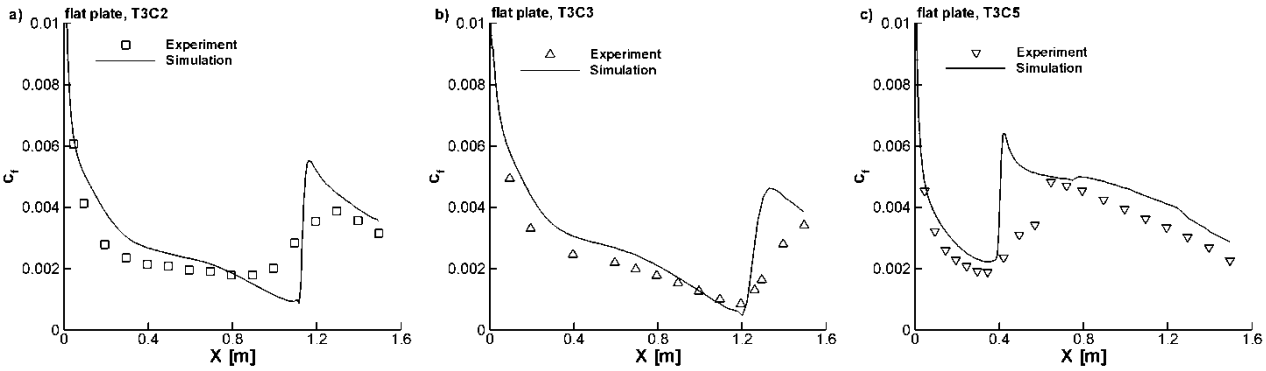

Fig. 2. Skin friction for variable-pressure gradient T3C flat plates.

ROLE OF THE THRESHOLD VALUE C_T AND THE DAMPING FACTOR f_{SS}

The roles of the onset parameter $k\omega/(\nu\Omega^2)$ in Eq. (7) and the turbulence penetration depth governed by the shear-sheltering factor f_{SS} (Eq. 4) are demonstrated in Fig. 3. The results were obtained for transition on the T106A profile with 3D URANS simulations with inlet turbulence *Tu* = 4 % (see later discussion). Fig. 3 shows cuts through the boundary layer on the suction side, in (a) the laminar, (b) transitional (prone to separation) and (c) fully turbulent zones, at the streamwise distances S/S_0 = 0.4, 0.7 and 0.9 (S_0 is the surface length on the suction side of the profile). The figure shows profiles of instantaneous velocity magnitude normalized by the velocity at the edge of the boundary layer, U/U_e, the onset parameter $k\omega/(\nu\Omega^2)$, the damping factor f_{SS} and small-scale, large-scale, and total turbulent kinetic energy. The vertical solid line shows the position where the threshold value of the onset parameter is reached (C_T = 0.1). For $k\omega/(\nu\Omega^2)$ < 0.1, near to the wall, the flow is treated as laminar. Production of turbulent kinetic energy is set to zero. For $k\omega/(\nu\Omega^2)$ > 0.1, production of turbulent kinetic energy is active, but it is damped by the shear-sheltering factor. A first observation is that the onset parameter $k\omega/(\nu\Omega^2)$ activates production relatively close to the wall inside the laminar boundary layer (above about y/δ = 0.2 in Fig. 3a). This is crucial for appropriate sensitivity to free-stream turbulence. The split between small- and large-scale turbulence is done by the damping factor f_{SS}. At the first position, the small-scale turbulent kinetic energy (k_s) does not penetrate very close to the wall (it is almost fully damped below y/δ = 0.4), so that the flow stays laminar near the wall. The peak value of k_l (associated with development of Klebanoff distortions) is visible at y/δ = 0.35 (but we do not use k_l for activation of transition in the current model). Farther downstream (Fig. 3b), transition to turbulence is activated by the nearer position to the wall of the threshold value of the onset parameter. The activation is visible by the small peak in the turbulent kinetic energy profile at distance y/δ = 0.35. The increase of the onset parameter in the near-wall zone has two causes. First, there is a slightly increased level of turbulent kinetic energy in the edge zone of the boundary layer due to upstream production and convection of the resulting turbulent kinetic energy. Second, the mean velocity profile is slightly inflectional by the adverse pressure gradient. This effect lowers the magnitude of the rotation rate near the wall. This way, the model reacts to a streamwise pressure gradient in the boundary layer. At the streamwise distance S/S_0 = 0.9 the flow is fully turbulent as shown in Fig. 3c. A strong peak of small-scale turbulent kinetic energy is produced around y/δ = 0.15. The large-scale turbulence (k_l) is pushed very near to the wall owing to small values of the damping factor f_{SS}. The peak value of k_l is about one order of magnitude smaller than the peak value of the small-scale turbulent kinetic energy k_s. The presence of k_l does almost not influence the small-scale turbulence profile.

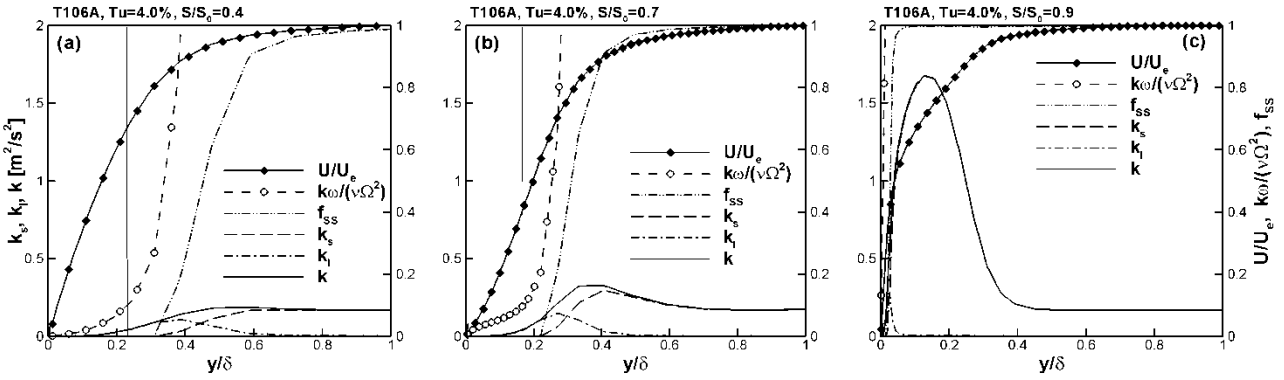

Fig. 3. Turbulence penetration mechanism of the model. 3D URANS simulation of flow over the T106A profile at Tu=4.0%; a) laminar, b) transitional and c) fully turbulent boundary layer states. In part (c) the small-scale turbulent kinetic energy profile (k_s) is on top of total turbulent kinetic energy profile (k).

TEST ON N3-60 CASCADE: BYPASS TRANSITION FAR FROM SEPARATION

We illustrate the performance of the model for transition in attached boundary layer state in steady 2D flow with the N3-60 profile, measured by Zarzycki and Elsner (2005). The N3-60 is the profile of a stator vane in the high-pressure part of a steam turbine. Geometric characteristics are: blade chord 300 mm, axial blade chord 203.65 mm, blade pitch 240 mm. The exit velocity is 30 m/s, which gives an exit Reynolds number of $6 \cdot 10^5$. The grid is similar to the grid of the T106A cacade shown later. It consists of 150,700 cells. The y^+ value of the first grid point in wall vicinity is below 0.35. At the inlet to the computational domain, placed at 0.52 times the axial chord upstream of the leading edge, a uniform flow with velocity U = 8.2m/s in axial direction was imposed. The inlet turbulence intensity was set to Tu = 3%. The inlet turbulent length scale was not reported in the measurements. In the simulations, the inlet turbulent length scale was adjusted by matching the measured turbulence intensity at distance 10 mm from the blade surface. The distance 10 mm is sufficiently far from the blade surface (above the boundary layer edge) so that this turbulence can be interpreted as local free-stream turbulence. The obtained turbulent length scale is L_t = 7mm. Fig. 4a shows a comparison between computed and measured turbulence intensity. The increased turbulence level from distance S/S_0 = 0.55 on is due to upstream turbulence generation in the shear layer on the suction side of the blade. This phenomenon is illustrated later for the T106A profile. The agreement is good which means that the inlet conditions for the modelled scalars have been set correctly. Fig. 4b shows a comparison between computed and measured shape factor H along the blade. The transition onset (S/S_0 = 0.75) and the growth rate in the transition region are reproduced correctly with the current model.

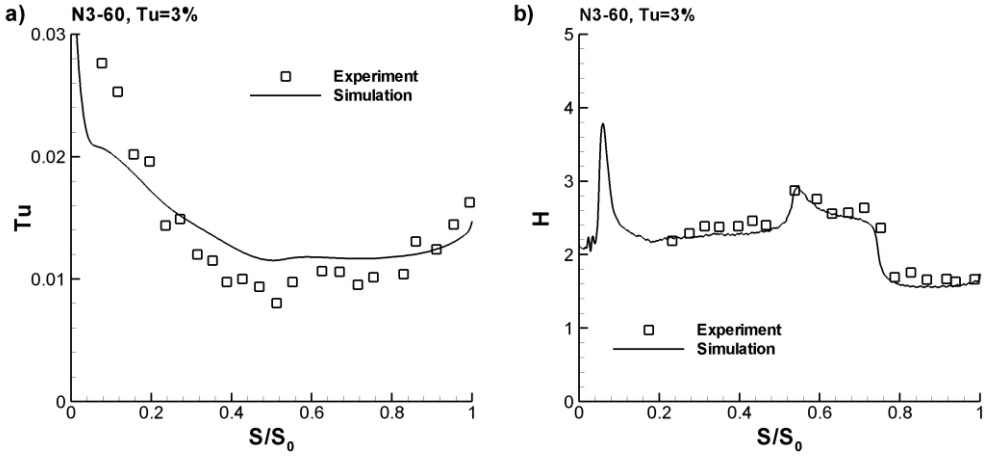

Fig. 4. N3-60 cascade, Tu=3%. Turbulence intensity along the suction side of the blade at distance 10 mm from the blade surface (a) and shape factor along the suction side of the blade (b).

TEST ON T106A CASCADE: BYPASS TRANSITION IN ATTACHED STATE PRONE TO SEPARATION AND TRANSITION IN SEPARATED STATE

Computations were performed on the T106A LP gas turbine blade cascade, measured by Opoka et al. (2008). Geometric characteristics are: blade chord 198 mm, axial blade chord 170 mm, blade pitch 158.2 mm. The measured inflow angle is 37.7º. The exit Reynolds number is $1.6\ 10^5$. Data are available for inflow turbulence Tu = 0.5% and Tu = 4% in the leading edge plane. Due to the rather low Reynolds number, laminar separation occurs at the suction side for Tu = 0.5%. The flow is prone to separation for Tu = 4%.

Both cases were simulated by time-accurate 3D URANS. A steady 2D RANS simulation was also done for Tu = 4%. The inlet to the computational domain was set at 0.62 times the axial chord upstream of the leading edge. The inflow angle was set to 39.7º, which is 2º more than in the experiments, in order to match the pressure distribution on the profile (not shown). The need for a

somewhat adjusted inlet angle comes from flow leakage through the slots of a bar-passing mechanism at the entrance to the cascade in the experiments. Table 3 summarizes the inlet conditions. For 2D RANS the grid consists of 72,000 cells, with a boundary layer grid near to the blade surface. The y^+ value in the first grid point in wall vicinity is below 0.3. An unstructured grid is added around the structured boundary layer grid. Fig. 5a shows a 2D cut of the 3D grid. The 3D grid for 3D URANS was generated by repeating the 2D grid in the spanwise direction. The size of the computational domain was set to $L_z = 0.20c$ in spanwise direction. This length was chosen based on the work of Lardeau et al. (2012), who performed LES of the flow over a compressor blade at a comparable Reynolds number by setting $L_z = 0.12c$. They showed that such a spanwise length is sufficient for resolving the three-dimensional instability and breakdown to turbulence of a separated laminar boundary layer. A somewhat larger spanwise length was chosen here, anticipating that 3D URANS may have a tendency to overestimate the size of the roll-up vortices in the spanwise direction at low free-stream turbulence (Tu = 0.5%), with respect to LES, due to larger numerical dissipation. So, we take into account that 3D URANS can resolve instability of a separated boundary layer, provided that the eddy viscosity by the turbulence model is set to a very low value. Actually, this then means functioning of 3D URANS as LES, which, of course, requires sufficient resolution in space and time and sufficient accuracy of the discretisation. Two grids were constructed, one with 1.1 million cells (denoted by 1M) and one with 4.8 million cells (denoted by 5M). The number of cells was set to 30 and 45 in the spanwise direction for the basic and fine meshes. The wall y^+ value is less than 0.8. The time step was selected so that the maximum CFL number was less than 2. At each time step, inner iterations were applied to lower the residuals of the momentum and the transport equations below 10^{-5}.

Table 3. T106A cascade. Boundary conditions at inlet to the computational domain. U denotes the velocity normal to the inlet boundary.

Test case	Simulation	U [m/s]	k [m^2/s^2]	ω [$1/s^2$]	L_t [m]
T106A (Tu=4.0%)	3D URANS	7.05	0.1443	603	0.007
T106A (Tu=0.5%)	3D URANS	7.05	0.0018	157	0.003
T106A (Tu=4.0%)	2D RANS	7.05	0.1443	603	0.007

There is no information in the experiments on the turbulent (integral) length scale. In the computations, the inlet values of the turbulent kinetic energy were adjusted (Table 3) such that the turbulence intensity at distance 10 mm from the suction-side blade surface in the leading edge plane was equal to 4.0% and 0.5%. The inlet turbulent length scale was estimated based on a series of 2D RANS simulations with Tu = 4.0%. Tests allowed to select a range of turbulent length scales for which the transition model shows strong sensitivity (L_t = 5-10mm). From this dataset we selected L_t = 7mm, which is the same turbulent length scale as used for the N3-60 profile. We have to accept that we cannot reproduce the inlet conditions with full confidence due to insufficient information about the experiments. A smaller turbulent length scale is needed with Tu = 0.5%, since in the experiments the turbulence grid was removed. We selected L_t = 3mm. But for Tu =0.5 %, results are not sensitive to turbulent length scale, as we show with Fig. 5b and the later Fig. 8b.

Fig. 5b shows the turbulence intensity at distance 10 mm from the suction-side blade surface. There is a strong increase of the turbulence level and final saturation of it for Tu = 0.5% and a slight increase of the turbulence level for Tu = 4.0% from distance S/S_0 = 0.2 on. These evolutions can be explained with Figs. 6 and 7 by contour plots of modelled and resolved turbulent kinetic energy. The turbulence production due to shear at the suction side of a blade, already starting at the leading

edge, is obvious in the modelled turbulent kinetic energy. The production and downstream convection of turbulent kinetic energy explain the slightly increasing turbulence level along the suction side with *Tu* = 4% (Fig 5b). The level varies from about 2.50 % to about 2.65 %. These values depend on the turbulence level in the inlet plane of the cascade, which is 4 %, and the turbulent length scale. It means that the turbulence level on the suction side of a blade is determined by both the oncoming turbulence from far upstream and the turbulence produced in vicinity of the suction side. The saturation level for *Tu* = 0.5 % is 0.5 %. This level is almost independent of the turbulent length scale, which means that it is dominantly determined by the production of turbulent kinetic energy in vicinity of the suction side. Further, we remark that there is almost no resolved turbulence for *Tu* = 4%, while it is significant in vicinity of the trailing edge for *Tu* = 0.5 %. We discuss the origin of the resolved turbulence hereafter.

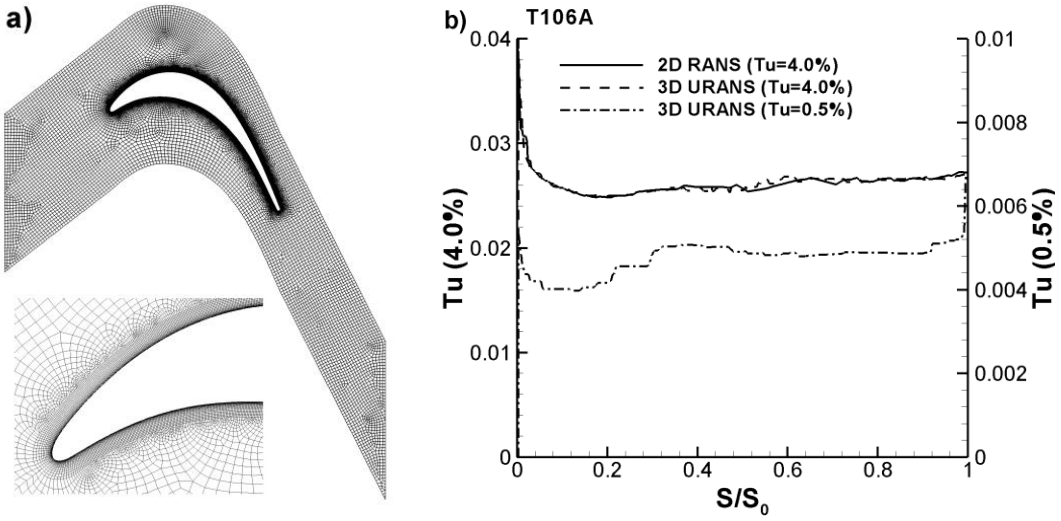

Fig. 5. Grid for simulations of the flow over T106A gas turbine profile (a). Turbulence intensity along the suction side at distance 10 mm from the blade surface for Tu=4.0% and Tu=0.5% (b).

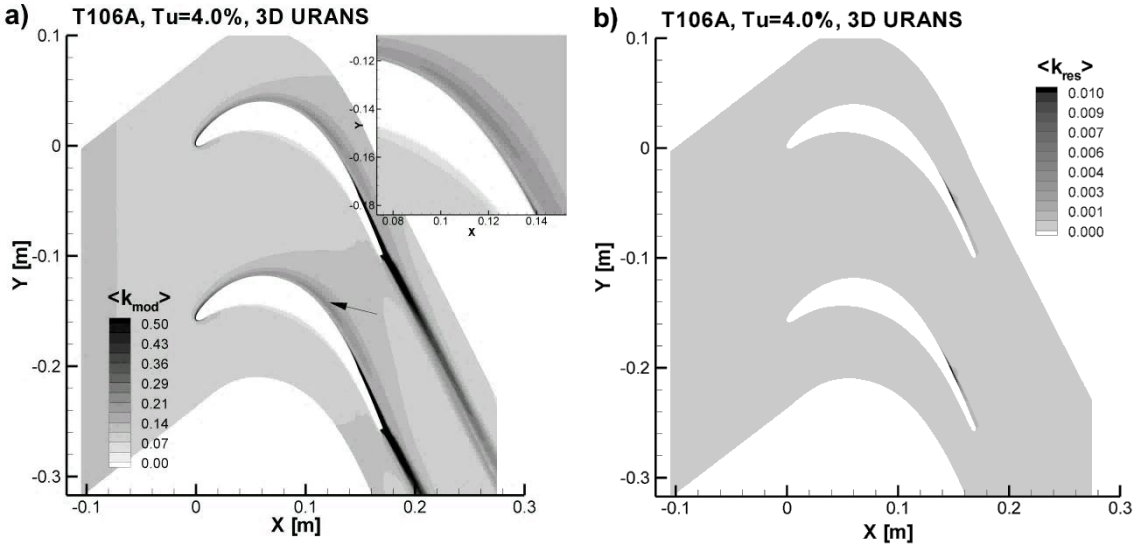

Fig. 6. T106A cascade, *Tu*=4.0%. 3D URANS. Time-averaged modelled turbulent kinetic energy (a) and time-averaged resolved turbulent kinetic energy (b) [m^2/s^2]. The magnified view in part (a) is the region indicated by the arrow.

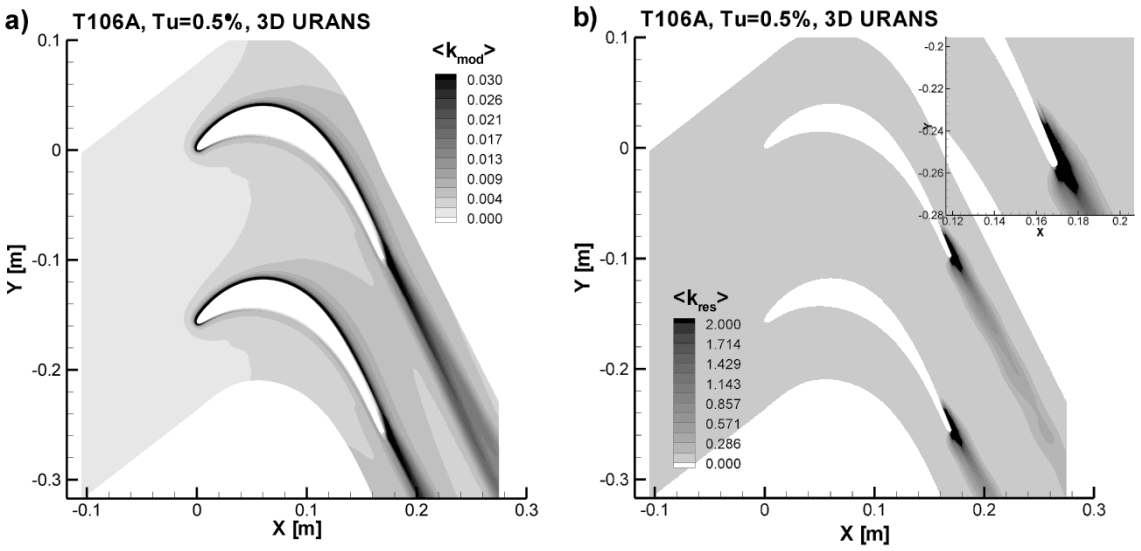

Fig. 7. T106A cascade, *Tu*=0.5%. 3D URANS. Time-averaged modelled turbulent kinetic energy (a) and time-averaged resolved turbulent kinetic energy (b) [m^2/s^2]. The magnified view in part (b) is the separated flow region near to the trailing edge.

The levels of time-averaged modelled (a) and resolved (b) turbulent kinetic energy in Fig. 7 for *Tu* = 0.5% are very different (take into account the much different scales in the figure parts). The level of modelled *k*, is low everywhere, compared to the level of resolved turbulence close to the trailing edge. Small values of modelled *k* are obtained outside the boundary layer, but the level is so small that the modelled turbulence is not able to trigger transition. In this case, the transition is obtained by resolved instability and onset of breakdown of the vortex structures originating from roll-up of the separated boundary layer. So nothing specific is done to trigger the transition. The success of the 3D URANS technique comes from setting the intermittency factor to zero in the near-wall zone over almost the whole length of the suction side. This means that the flow near the wall is represented as laminar and that separation of the laminar boundary layer can be obtained. Instability and onset of breakdown of the separated layer are resolved in vicinity of the trailing edge. The factor C_K in the Kolmogorov time scale (Eq. 6) is crucial for success and was tuned with this case. The constant has been selected taking into account two limits. On one hand, a too small value of C_K leads to too strong decay of the free-stream turbulence and to massive flow separation and delayed transition. On the other hand, a too large value of C_K leads to overproduction of turbulent kinetic energy in the stagnation flow region. Figs. 6a and 7a show that there is no spurious generation of turbulent kinetic energy in the stagnation flow region. It means that the C_K constant has been set properly.

Fig. 8a shows the shape factor on the suction side obtained with 2D RANS and 3D URANS for *Tu* = 4%. The transition is of bypass type but the flow is prone to separation. The time-accurate 3D URANS simulations were performed on the basic and fine grids with 1 and 5 million (M) cells. Both results are in good agreement with the experiments and are also close to each other. This means that grid-independent results have been obtained on the basic grid. 2D RANS results are somewhat off. This is due to a somewhat larger turbulent length scale produced in 2D RANS in the rear part of the blade (result not shown). As a result, the transition onset is predicted somewhat too early with 2D RANS. It was verified that deactivation of the transition model (simulation of fully turbulent boundary layer flow) does not lead to a significant change of the eddy viscosity level above the boundary layers. It means that differences between results of 2D RANS and 3D URANS (Fig. 8a) are due to different behaviour of the underlying turbulence model, and are not much influenced by the transition model.

Fig. 8b shows the comparison of the shape factor from measurements and computations with 3D URANS at low free-stream turbulence (Tu = 0.5%). In this case, the transition occurs in the separated laminar boundary layer. Numerically, the boundary layer separates somewhat too late in comparison with the experiments (around S/S_0 = 0.75), but the transition to turbulent flow is reproduced well. In this case, the intermittency factor γ is very low in the boundary layer along the full length of the suction side (not shown). It means that the role of the transition model is shielding the laminar and separated parts of the boundary layer from free-stream disturbances. Fig. 8b shows that reducing the turbulent length scale from 3 to 1 mm results in almost no change in the shape factor distribution. It means again that the transition comes from resolved instability of the separated shear layer. In this case, the role of the underlying turbulence/transition model is much less than in the high turbulence case. It also means that in flows with strong laminar boundary layer separation at low freestream turbulence a change to the inlet turbulent length scale has less influence on the transition onset location than in the attached boundary layer flows. The above results indicate that 2D URANS and 2D RANS cannot be successful with transition in separated state, since 2D simulations cannot detect three-dimensional instability and breakdown.

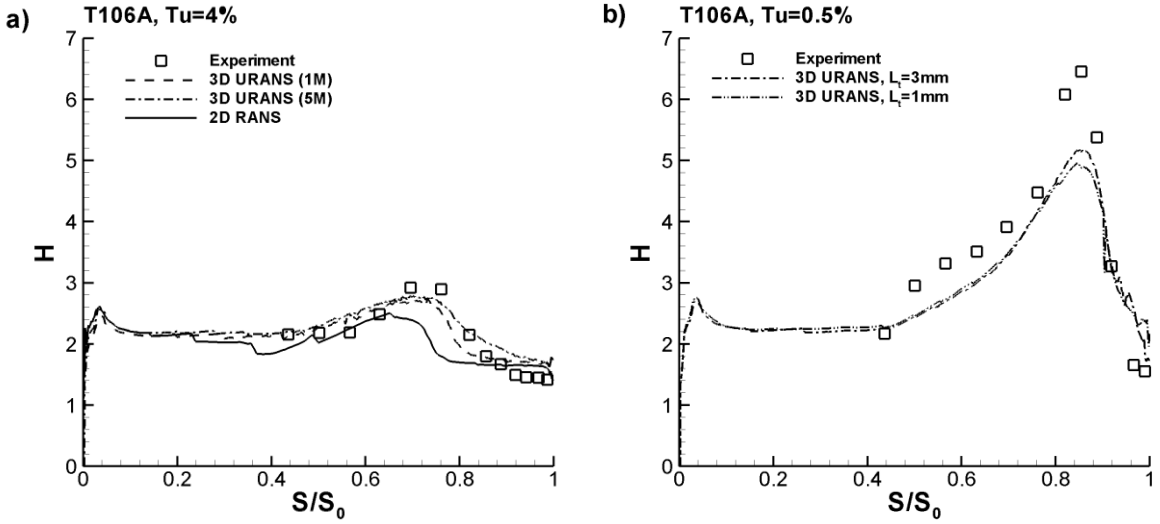

Fig. 8. T106A cascade. Shape factor along the suction side. Tu=4 % (a) and Tu=0.5% (b).

CONCLUSIONS

An algebraic intermittency model has been derived for simulation of bypass transition. The model is coupled with the newest version of the k-ω RANS turbulence model by Wilcox (2008). The model is based on local variables and does not require computation of the wall distance.

The model gives good results for transition in boundary layers in attached state (N3-60 cascade, Tu = 3%), state prone to separation (T106A cascade, Tu = 4%) and separated state (T106A cascade, Tu = 0.5%). The 3D URANS technique was found to be successful for transition simulation in a separated laminar boundary layer at low free-stream turbulence level owing to its ability to resolve the instability of the vortex structures in the separated shear layer.

ACKNOWLEDGEMENT

The first two authors acknowledge support from a research project funded by the Polish National Science Centre (contract number UMO-2011/01/B/ST8/07267). The authors are grateful for access to the computer resources in Gdansk, made available by the Pl-Grid community.

REFERENCES

Brandt L., Schlatter P., Henningson D.S. (2004), *Transition in boundary layers subject to free-stream turbulence*, J. Fluid Mech. 517:167-198.

Jacobs. R.G., Durbin P.A. (2001), *Simulations of bypass transition*, J. Fluid Mech. 428:185-212.

Kubacki S., Lodefier K., Zarzycki R., Elsner W., Dick E. (2009), *Further development of a dynamic intermittency model for wake-induced transition*, Flow, Turbulence Combust. 83:539-568.

McAuliffe B.R., Yaras M.I. (2010), *Transition mechanisms in separation bubbles under low- and elevated freestream turbulence*, J. Turbomachinery 132:011004/1-10.

Langtry R.B., Menter F.R. (2009), *Correlation-based transition modeling for unstructured parallelized computational fluid dynamics codes*, AIAA J. 47:2894-2906.

Lardeau S., Leschziner M., Li N. (2004), *Modelling bypass transition with low-Reynolds number non-linear eddy-viscosity closure*, Flow, Turbulence Combust. 73:49-76.

Lardeau S., Leschziner M., Zaki T. (2012), *Large eddy simulation of transitional separated flow over a flat plate and a compressor blade*, Flow, Turbulence Combust. 88:19-44.

Lodefier K., Dick E. (2006), *Modelling of unsteady transition in low-pressure turbine blade flows with two dynamic intermittency equations*, Flow, Turbulence Combust. 76:103-132.

Opoka M.M, Thomas R.L., Hodson H.P. (2008), *Boundary layer transition on the high lift T106A low-pressure turbine blade with an oscillating downstream pressure field*, J. Turbomachinery, 130:021009/1-10.

Praisner T.J., Clark J.P. (2007), *Predicting transition in turbomachinery - Part 1: a review and new model development*, J. Turbomachinery, 129:1-13.

Walters D.K., Leylek J.H. (2004), *A new model for boundary layer transition using a single-point RANS approach*, J. Turbomachinery 126:193-202.

Walters D.K., Cokljat D. (2008), *A three-equation eddy-viscosity model for Reynolds-averaged Navier-Stokes simulations of transitional flow*, J. Fluids Engineering 130:12401/1-14.

Walters. K. (2009), *Physical interpretation of transition-sensitive RANS models employing the laminar kinetic energy concept*, Ercoftac Bulletin 80:67-76.

Wilcox D.C. (2008), *Formulation of the k-ω turbulence model revisited*. AIAA J., 46:2823-2837.

Zarzycki R., Elsner W. (2005), *The effect of wake parameters on the transitional boundary layer on a turbine blade*, IMechE Part A, J. Power and Energy, 219:471-480.

Zaki. T. A., Durbin P.A. (2005), *Mode interaction and the bypass route to transition*, J. Fluid Mech. 531:85-111.